Title

Surface-Plasmon-Assisted Photoelectrochemical Reduction of CO_2 and NO_3^- on Nanostructured Silver Electrodes

Journal

Advanced Energy Materials, 8(22)

ISSN

1614-6832

Authors

Kim, Y
Creel, EB
Corson, ER
et al.

Publication Date

2018-08-06

DOI

10.1002/aenm.201800363

Peer reviewed

Surface-Plasmon-Assisted Photoelectrochemical Reduction of CO_2 and NO_3^- on Nanostructured Silver Electrodes

*Youngsang Kim, Erin B. Creel, Elizabeth R. Corson, Bryan D. McCloskey, Jeffrey J. Urban, and Robert Kostecki**

Electrochemical reduction of carbon dioxide (CO_2) typically suffers from low selectivity and poor reaction rates that necessitate high overpotentials, which impede its possible application for CO_2 capture, sequestration, or carbon-based fuel production. New strategies to address these issues include the utilization of photoexcited charge carriers to overcome activation barriers for reactions that produce desirable products. This study demonstrates surface-plasmon-enhanced photoelectrochemical reduction of CO_2 and nitrate (NO_3^-) on silver nanostructured electrodes. The observed photocurrent likely originates from a resonant charge transfer between the photogenerated plasmonic hot electrons and the lowest unoccupied molecular orbital (MO) acceptor energy levels of adsorbed CO_2, NO_3^-, or their reductive intermediates. The observed differences in the resonant effects at the Ag electrode with respect to electrode potential and photon energy for CO_2 versus NO_3^- reduction suggest that plasmonic hot-carriers interact selectively with specific MO acceptor energy levels of adsorbed surface species such as CO_2, NO_3^-, or their reductive intermediates. This unique plasmon-assisted charge generation and transfer mechanism can be used to increase yield, efficiency, and selectivity of various photoelectrochemical processes.

Dr. Y. Kim, E. B. Creel, E. R. Corson, Prof. B. D. McCloskey, Dr. J. J. Urban, Dr. R. Kostecki
Joint Center for Artificial Photosynthesis
Lawrence Berkeley National Laboratory
Berkeley, CA 94720, USA
E-mail: r_kostecki@lbl.gov

E. B. Creel, Dr. J. J. Urban
The Molecular Foundry
Lawrence Berkeley National Laboratory
Berkeley, CA 94720, USA

E. B. Creel
Department of Chemistry
University of California
Berkeley, CA 94720, USA

E. R. Corson, Prof. B. D. McCloskey
Department of Chemical and Biomolecular Engineering
University of California
Berkeley, CA 94720, USA

Prof. B. D. McCloskey, Dr. R. Kostecki
Energy Storage and Distributed Resources Division
Lawrence Berkeley National Laboratory
Berkeley, CA 94720, USA

1. Introduction

One proposed mechanism to actively mitigate climate change is the capture and sequestration of carbon dioxide (CO_2) to reduce atmospheric greenhouse gas concentrations. However, the impact of this approach is multiplied if CO_2 could be treated as a chemical feedstock rather than a waste byproduct. Fundamentally, this is possible—CO_2 can be converted to a variety of carbon-based chemicals through reduction processes, the most promising of which is direct conversion to ethanol and other oxygenates.[1–3] However, while there are several methods to chemically reduce CO_2—e.g., using electrochemical, photochemical, and biological methods—none have achieved both high efficiency and selectivity.

Electrochemical CO_2 reduction in aqueous electrolytes competes with hydrogen evolution and suffers from high overpotentials and low selectivity for highly reduced products such as hydrocarbons and alcohols. Moreover, the products formed in CO_2 reduction depend sensitively on the cathode composition. While formate ($CHOO^-$) is the primary product at many metal electrodes,[4,5] silver (Ag) and gold (Au) chiefly promote the formation of carbon monoxide (CO).[5,6] Copper (Cu) is unique among the metals as a catalyst for CO_2 electroreduction because it yields multiple commercially valuable products, including methane, ethylene, and ethanol.[1,7,8]

Although some metal electrodes have proven selective CO_2 reduction to formate or CO (a valuable Fischer-Tropsch feedstock), they tend to operate at high overpotentials, which decreases energy efficiency and selectivity versus the hydrogen evolution reaction.[4–6] An effective way to lower the kinetic barrier for CO_2 reduction is photoactivation by modifying the binding energy of the adsorbed reaction intermediates and/or by facilitating charge transfer via photoexcited charge carriers. Silver is particularly well suited for such photoactivation because the excitation of surface plasmons at this metal occurs at 3.6 eV (344 nm) and overlaps with the solar spectrum.[9,10] By altering the size and shape of nanoscale features in Ag electrodes, their plasmon resonance can be tuned throughout the UV–vis–NIR region,[10] which is easily accessible to optical measurements.

Previous studies have shown that plasmonically excited hot-carriers[11,12] can be injected into the molecular orbitals (MOs) of nearby acceptors.[3,4,7,13] Precisely designed and engineered nanostructures exhibiting strong localized surface plasmon resonances (LSPR) have been used as well-defined photocatalysts to promote the hot-carrier-assisted mechanism of hydrogen dissociation[14,15] and water splitting.[9,16] Plasmonic hot-carrier excitation and emission along with the strong local electric fields produced by surface plasmons on Ag may open new mechanistic pathways for CO_2 reduction by altering the interaction between the electrode surface and electron acceptor species such as adsorbed CO_2 and $COOH_{ads}$.[17,18] In fact, early reports by Kostecki and Augustynski[19–21] revealed the existence of unusually large steady-state cathodic photo-currents on illuminated roughened Ag electrodes in CO_2-saturated or nitrate (NO_3^-)-containing aqueous solutions. These roughened Ag electrodes exhibit a sharp photoemissive yield maximum at 3.6 eV corresponding to the surface plasmon resonance energy in Ag. Illumination of the Ag electrode with a broadband UV–vis light source reduced the overpotential of CO_2 reduction by ≈0.5 V and significantly increased the rate and faradaic efficiency (FE) of CO formation. It has been postulated that these beneficial effects result from the photoexcitation of surface plasmons that then decay to produce excited ("hot") electrons and holes in the vicinity of the Ag sur-face.[10,11] However, the exact mechanism of plasmon-assisted electrochemical reduction of CO_2 or NO_3^- remains unknown.

2. Photoelectrochemical Reduction of CO_2

Although photoelectrochemical CO_2 reduction on an electrochemically roughened Ag electrode in aqueous electrolytes has been demonstrated,[20,21] a more precisely defined Ag electrode surface morphology is required to understand the mechanism of photocurrent generation and the nature of electrode-adsorbate interactions. In this study, electrodes with two sizes of hexago-nally arrayed 180 or 75 nm Ag nanopyramids (AgPyr) (**Figure 1**) were fabricated using nanosphere lithography[22] (see the Experi-mental Section and the Supporting Information for technical details related to electrode fabrication, photoelectrochemical, and UV–vis total reflectance measurements). Finite element method (FEM) simulations of the LSPR on the Ag pyramids show that upon optical excitation, the electric field is maximized at the apex of the nanopyramids (Figure 1e,f and Figure S3, Supporting Information). The photocatalytic activity of the illuminated Ag nanopyramids used for photoelectrochemical reduction of CO_2 or NO_3^- was compared to a smooth (Ag film deposited on glass) and an electrochemically roughened Ag foil electrode.[20,21] Electro-chemically roughened Ag and 180 nm AgPyr have similar rough-ness factors whereas 75 nm AgPyr has significantly higher surface area than the other three electrodes as determined by double layer capacitance measurements (Table S1, Supporting Information).

2.1. Linear Sweep Voltammetry (LSV)

Current density (J, current per geometric surface area of the electrode) was measured as a function of potential for the "dark" and illuminated Ag electrodes during a LSV scan, using near-UV–vis light chopped at 3 Hz (**Figure 2**). A square wave current response is the result of the photocurrent generation upon the intermittent illumination (Figure S5, Supporting Information). Of note, the "dark" current and photocurrent profiles were reproducible and stable over time for all the electrodes (Figure S7, Supporting Information). Interestingly, the overall current (J) in the Ar-saturated electrolyte is much higher than in the presence of CO_2 (Figure 2a), indicating that the ongoing reduction of CO_2 results in suppression of the hydrogen evolution reaction via possible high surface coverage of CO_2 or reduction intermediates. Moreover, the observed current densities are not directly proportional to the surface roughness, implying that vigorous mechanical stirring and continuous gas bubbling of CO_2 through the electrolyte could be responsible for the observed current inconsistency during the LSV measurements.

The photocurrent density (J_{ph}) in CO_2-saturated electrolyte was extracted from the overall current during the LSV scans (Figure 2b) by using a lock-in amplifier synchronized with the frequency of the light chopper. The photocurrent observed at all four Ag electrodes exhibits a maximum at −1.1 V versus reversible hydrogen electrode (RHE). Interestingly, the J_{ph} peak potential coincides with the maximum Faradaic efficiency of CO formation at the silver electrode in dark conditions,[23] suggesting that the plasmonic hot-carriers contribute to the electroreduction of CO_2 and formation of CO.

The maximum J_{ph} on the 75 nm AgPyr electrode is significantly higher than on the other Ag electrodes (**Table 1**). Intriguingly, the photocurrent on the 180 nm AgPyr is twice that of the electrochemically roughened Ag, although their roughness factors are similar. Additionally, the magnitude of J_{ph} at −1.1 V observed on the 75 nm AgPyr electrode makes up a larger fraction (≈30%) of the overall current than the J_{ph} on the other electrodes (Table 1). This observation suggests that the specific size and geometry of the well-defined pyramid nanostructures is the origin of the enhanced photocurrent from the AgPyr samples (as compared to the random features on roughened Ag), in line with our hypothesis that these pyramidal structures should be plasmonically active.

The observed "resonant-like" behavior of J_{ph} at −1.1 V could be associated with the surface plasmon-enhanced hot-electron generation and the surface coverage and binding strength of adsorbed reactants (H_2O, H_3O^+, CO_2) or reaction intermediates (e.g., CO_2^-, COOH, $C(OH)_2^-$, COH, and CH=O)[24] as a function of applied potential. LSV measurements on the Ag nanopyramid electrodes in Ar-saturated electrolyte with no CO_2 present show that J_{ph} is negligible compared to similar measurements in a CO_2-saturated electrolyte (Figure 2b). The significant decrease of the photocurrent in the absence of CO_2 and its overlap with the CO formation rate in the presence of CO_2[23] indicate that the photocurrent is primarily related to CO_2 rather than water reduction. This implies that either adsorbed CO_2 or related adsorbed intermediate species are the likely hot electron scavengers that contribute to the observed photocurrent. This observation is also consistent with the observed shift of the J_{ph} onset from −0.75 V for the smooth Ag electrode to −0.32 V for 75 nm AgPyr (Figure 2b), which indicates a notable decrease in CO_2 reduction overpotential.[25] The reduction in J_{ph} onset potential upon illumination is likely a result of two plasmonic effects: 1) The improved generation of excited

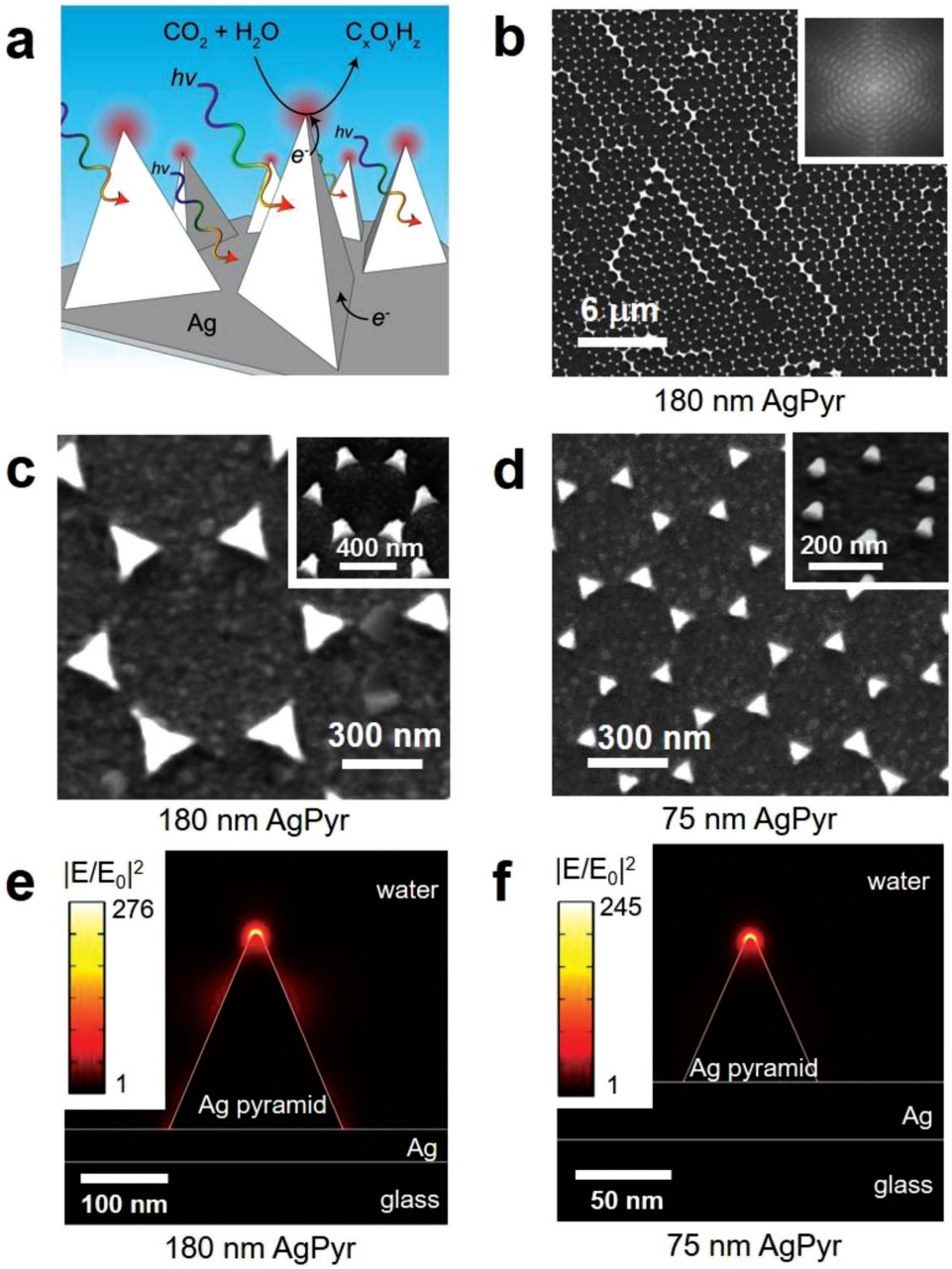

Figure 1. Ag nanopyramid electrodes. a) A graphic depiction of photoelectrochemical reduction on plasmonically active Ag nanopyramids. b) Scanning electron microscopy (SEM) image of a 180 nm AgPyr electrode. Inset shows the fast Fourier transform (FFT) of the SEM image to confirm the periodicity. SEM images of c) 180 nm AgPyr and d) 75 nm AgPyr. The insets show 45° tilted SEM images. Local electric field distributions ($|E/E_0|^2$) simulated by finite element method (COMSOL) are shown for e) 180 nm AgPyr at 650 nm and f) 75 nm AgPyr at 350 nm.

electrons with sufficient energy to be injected into surface adsorbed species at lower overpotentials and 2) surface-plasmon-induced localized enhancements in electric fields at locations where charge injection occurs (i.e., at the pyramid tips).

2.2. Incident Photon-to-Current Efficiency (IPCE)

To understand the effect of plasmonic hot-electrons on the mechanism of electrochemical CO_2 reduction, IPCE as a Scanning Electron Microscopy function of applied potential and incident light wavelength was measured in CO_2- and Ar-saturated 0.1 M $NaClO_4$ aqueous electrolyte. IPCE measurements in Ar-saturated electrolyte showed negligible photocurrent (Figure S10, Supporting Information). The IPCE plots for both 180 nm AgPyr and 75 nm AgPyr electrodes measured in CO_2-saturated electrolyte (**Figure 3**) exhibit a resonant peak at 360–380 nm, i.e., in the range of energies corresponding to surface plasmons on silver, as it was previously observed on a roughened silver electrode.[21] This is supported by the absorbance spectrum

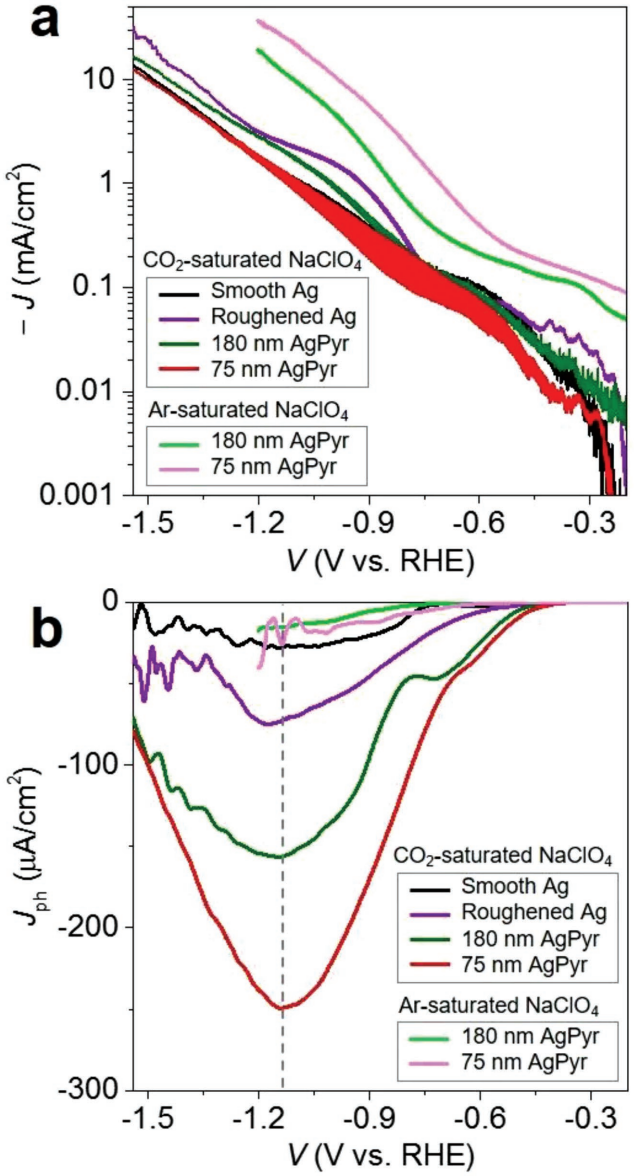

Figure 2. Total cathodic current (J) and photocurrent densities (J_{ph}) in CO_2- or Ar-saturated 0.1 M $NaClO_4$. a) J and b) J_{ph} under modulated illumination (3 Hz) on smooth Ag, roughened Ag, 180 nm AgPyr, and 75 nm AgPyr electrodes. Cathodic sweep rate was 5 mV s^{-1} for all measurements.

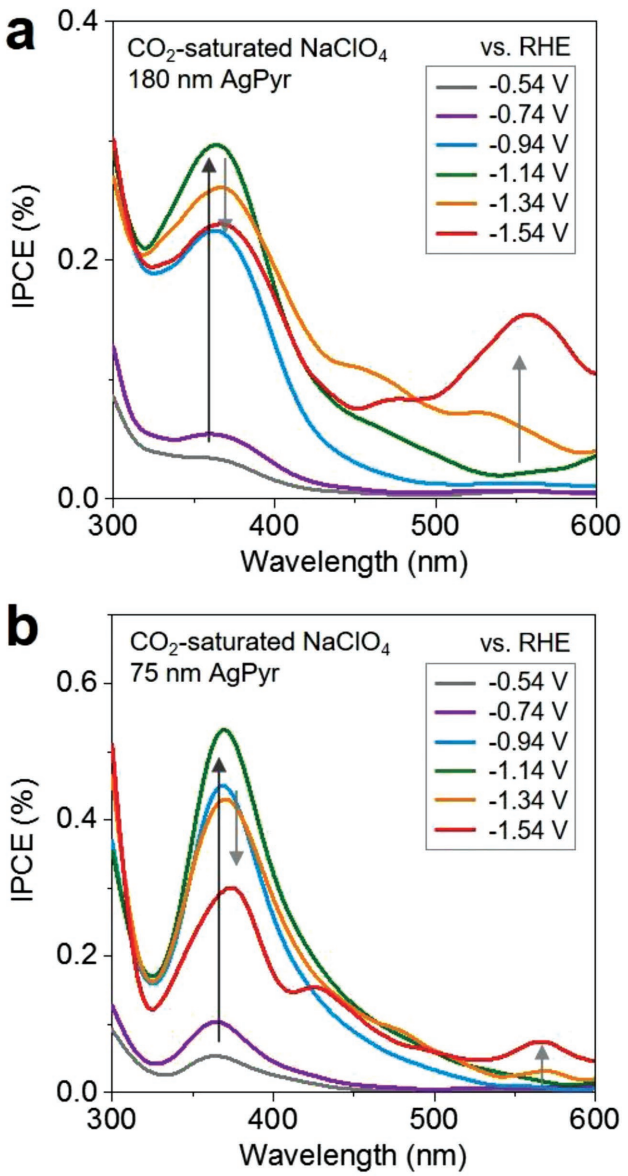

Figure 3. IPCE measured as a function of applied potential in CO_2-saturated 0.1 M $NaClO_4$. IPCE measurements were performed in CO_2-saturated $NaClO_4$ for a) 180 nm AgPyr and b) 75 nm AgPyr. The arrows indicate the increase and decrease in IPCE amplitudes at 360 and 550 nm with decreasing electrode potential.

of a 75 nm AgPyr electrode shown in Figure S10 in the Supporting Information. The intensity of the IPCE peak at 360 nm increases as the potential becomes more negative, reaching a maximum at –1.1 V, after which it decreases at more negative potentials. Note that the potential maximum for the 360 nm peak matches the potential maxima for the overall photocurrent and for CO production. Thus, the 360 nm peak in the IPCE is likely attributed to CO generation.

Table 1. CO_2 reduction activity metrics at –1.1 V versus RHE.

Electrode	Dark current density, J [mA cm^{-2}]	Photocurrent density, J_{ph} [mA cm^{-2}]	J_{ph}/J
Smooth Ag	–1.1	–0.03	2.5%
Roughened Ag	–2.2	–0.07	3.2%
180 nm AgPyr	–1.7	–0.15	8.8%
75 nm AgPyr	–0.8	–0.25	29%

At potentials more cathodic than –1.1 V, the peak at 360 nm shifts slightly toward longer wavelengths and another major peak emerges at 550 nm for both nanopyramid electrodes along with additional peaks either at 430 nm for the 75 nm AgPyr electrode or 470 nm for the 180 nm AgPyr electrode (Figure 3). We attribute the emergence of these new peaks at potentials more negative than –1.1 V to the likely formation and subsequent

photoreduction of new intermediates upon further reduction of CO. Previous reports of dark CO_2 reduction at smooth Ag electrodes at these potentials observed the formation of small amounts of methane (CH_4), methanol (CH_3OH), or ethanol (C_2H_5OH) through the transient intermediates $CH{=}O_{ads}$ and $C{-}OH_{ads}$.[23,26] The IPCE peaks at 430, 470, and 550 nm could be related to photoassisted hot-electron injection into these adsorbates. Our observations from IPCE measurements indicate that the photon energy level at which excited charge injection occurs is dependent on three factors: 1) the electrode's plasmon resonance energy, 2) the MO energies of the surface acceptors (e.g., CO_2 or reaction intermediates), and 3) the electrode potential.

3. Photoelectrochemical Reduction of NO_3^-

To further validate the importance of these factors on excited charge injection from a photoelectrode to an adsorbate, a series of similar experiments at AgPyr photoelectrodes was performed in the presence of NO_3^- ions, which are effective acceptors of photogenerated excited electrons in electrochemical systems.[20,27] The cathodic currents (>100 mA cm^{-2} at −1.1 V, inset of **Figure 4**a) that correspond to NO_3^- reduction to NO_2^- are more than two orders of magnitude higher that the CO_2 reduction current (≈1 mA cm^{-2} at −1.1 V, Figure 2a). This is easily rationalized by the relatively high concentration of NO_3^- (1 M) in the electrolyte compared to the saturated concentration of CO_2 (≈30×10^{-3} M) in the 1 M $NaClO_4$ aqueous electrolyte. On the other hand, photocurrents measured on AgPyr electrodes in 1 M $NaNO_3$ electrolyte (Figure 4a) are of the same magnitude as those observed in the CO_2-saturated electrolyte (Figure 2b). Interestingly, the photocurrent observed in the NO_3^- solution displays two maxima at −1.0 and −1.2 V. The resulting product at −1.0 V is nitrite (NO_2^-) with near 100% FE, as determined by titration analysis[28] (see the Supporting Information for description of titration analysis), which is in good agreement with the results from earlier reports.[29,30] The photocurrent peak at −1.2 V is likely related to production of nitric oxide (NO) or NH_4^+ on silver.[30]

IPCE measurements in the NO_3^--containing electrolyte on the 180 nm AgPyr and 75 nm AgPyr electrodes lack the resonant peak at 360 nm, which was clearly observed in the CO_2-saturated electrolyte (Figure 4b,c). In fact, new maxima emerge at 400, 530, and 620 nm for both AgPyr electrodes, with the peak intensity varying significantly with the applied potential. The new peaks likely correspond to the MOs of adsorbates related to NO_3^- reduction, which are at different energy levels than CO_2 intermediates. The distinct difference between photoactive wavelengths in CO_2 and NO_3^- reduction confirms that the resonant-like behavior depends not only on the plasmon resonance of the Ag electrodes but also on the chemical nature of the hot-electron acceptors present at the electrode surface and the excited electronic states generated upon illumination.

4. Plasmon-Generated Charge Carrier Injection Mechanism at Potential-Biased Electrodes

Photoelectrochemical reduction measurements in the same electrolyte with the addition of CO_2 or NO_3^- yield notable

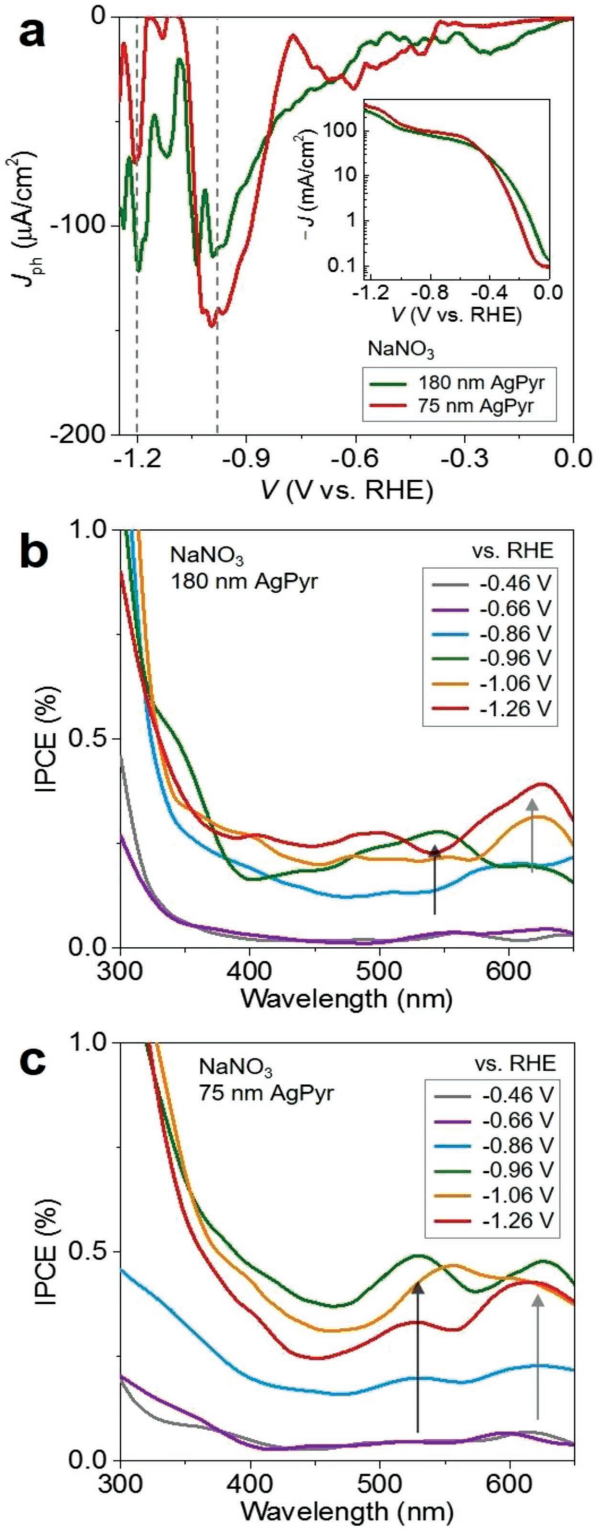

Figure 4. Photocurrent densities (J_{ph}) and IPCE in 1 M $NaNO_3$. a) J_{ph} measured in 1 M $NaNO_3$ at 180 nm AgPyr (green) and 75 nm AgPyr (red) electrodes. Inset shows current density (J) as a function of the applied potential under modulated illumination (3 Hz). 5 mV s^{-1} sweep rate was used. IPCE was measured in 1 M $NaNO_3$ for b) 180 nm AgPyr and c) 75 nm AgPyr as a function of applied potential.

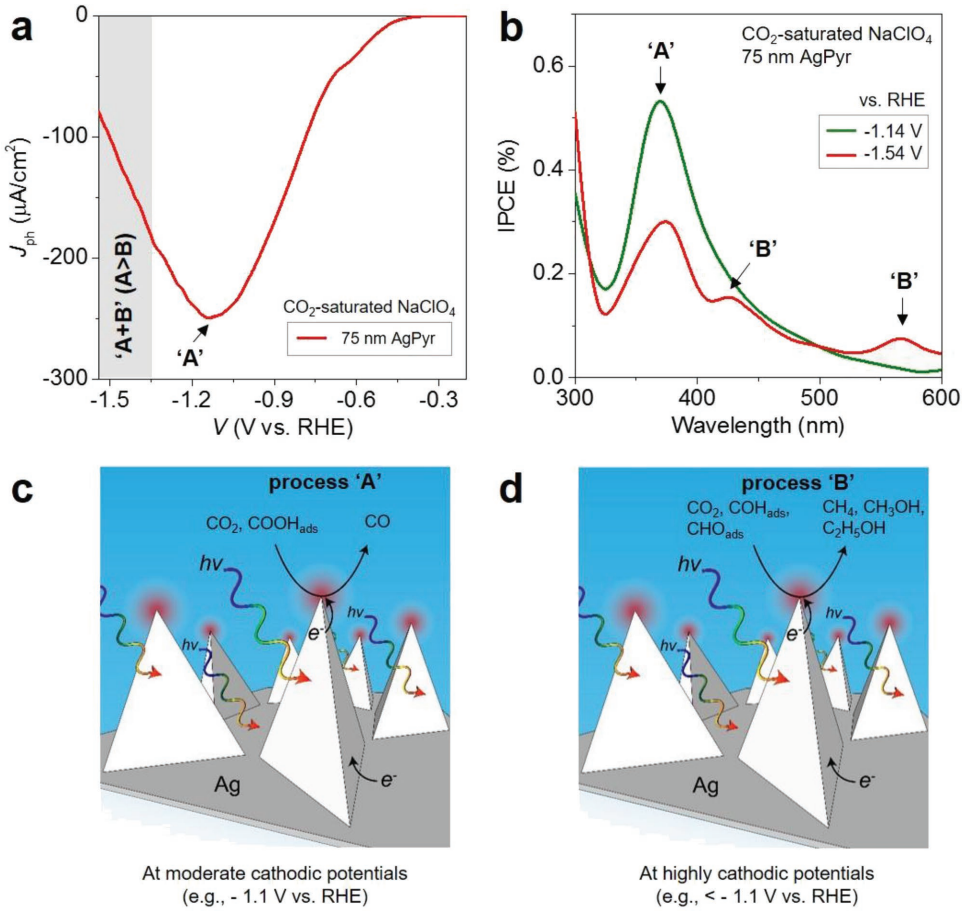

Figure 5. Photoelectrochemical reduction of CO_2 at different applied potentials. a) Photocurrent density (J_{ph}) in CO_2-saturated 0.1 M $NaClO_4$ on 75 nm AgPyr electrode is shown. The resonant photocurrent at ≈– 1.1 V versus RHE corresponds to process "A," shown schematically in panel (c). The shaded area at highly cathodic potential corresponds to the combination of processes "A" and "B," where "B" is a minor process shown in panel (d). b) IPCE measured in CO_2-saturated $NaClO_4$ on 75 nm AgPyr at –1.14 and –1.54 V versus RHE is demonstrated. Process "A" occurs at ≈360 nm and moderate cathodic potentials. Process "B" occurs at longer wavelengths (>360 nm) and highly cathodic potentials. c) In process "A," the hot-carriers inject into $CO_{2\ ads}$ or $COOH_{ads}$ at moderate cathodic potentials. d) In process "B," the hot-carriers inject into $CO_{2\ ads}$, COH_{ads}, or CHO_{ads} at highly cathodic potentials.

photocurrents, indicating that the plasmonic activity is selective toward the high-activation-barrier CO_2 and NO_3^- reduction reactions rather than water reduction. At cathodic potentials (**Figure 5**) we hypothesize that plasmonically excited hot-electrons can be injected into MOs of acceptor molecules or intermediates, which are present only on the Ag electrode surface. The proposed resonant injection would occur when the energy of hot-electrons—tuned by the applied potential—aligns with the energy of the MO, analogous to the mechanism of a resonant tunneling diode. Of course, this resonant potential depends on the energy levels of the acceptor molecule, explaining why the resonant potentials and wavelengths are different for each target of photocatalytic reduction, i.e., – 1.1 V and 360 nm for CO_2 reduction and –1.0, –1.2 V, 530 nm, and 620 nm for NO_3^- reduction. Each molecule will have its own unique attendant cascade of reductive intermediates, each with their own characteristic energy levels.

The two-electron reduction of CO_2 to CO and NO_3^- to NO_2^- both happen with an initial slow electron transfer followed by a second fast electron transfer[17,18,23,31]

$$CO_{2\,ads} + H^+ + e^- \rightarrow COOH_{ads}\ (\text{slow}) \quad (1a)$$

$$COOH_{ads} + H^+ + e^- \rightarrow CO + H_2O\ (\text{fast}) \quad (1b)$$

$$NO_{3\,ads}^- + H^+ + e^- \rightarrow HNO_{3\,ads}^-\ (\text{slow}) \quad (2a)$$

$$HNO_{3\,ads}^- + H^+ + e^- \rightarrow NO_2^- + H_2O\ (\text{fast}) \quad (2b)$$

At highly cathodic potentials, the electron transfer rate to CO and NO_2^- becomes competitive with their desorption rates,[23] thereby allowing further reduced products to be formed. The additional IPCE peaks that appear at potentials <–1.2 V correspond to subsequent (>2) electron transfer and formation of CH_4, CH_3OH, and C_2H_5OH or NO, N_2, and NH_4^+ for CO_2 and NO_3^- reduction, respectively.[23,26,30] CO and NO_2^- together with NO or carbene (COH_{ads})[23] become intermediates in this extended reaction pathway toward these new reduction products[3,17,30] (Figure 5b). While we cannot currently confirm the identity of

charge acceptor species during photoreduction of either CO_2 or NO_3^-, our IPCE data are most consistent with charge injection into adsorbed reductive intermediates, whose surface coverage change with applied voltage, rather than directly into CO_2 or NO_3^-. Future spectroscopic studies to identify these species are certainly warranted to confirm our hypothesized mechanism for charge injection.

5. Conclusion

We hypothesize that plasmonically excited hot-electrons are injected into specific unoccupied MOs of intermediate acceptors depending on the applied potentials and the energy of hot-electrons as depicted in Figure 5, resulting in selective reduction reactions.[32] The distinct differences in the observed resonant effects at the Ag electrode with respect to electrode potential and photon energy for CO_2 versus NO_3^- reduction systems strongly support the proposed contention that plasmon-enhanced photoelectrochemical reduction of these species is dominated by the relationship between the electronic structure of the acceptor molecules and catalyst. The experimental results suggest that plasmonic hot-carriers indeed interact selectively with specific MO energies of acceptors, which could include adsorbed CO_2, NO_3^-, or their intermediates such as $COOH_{ads}$ and $HNO_3^-{}_{ads}$. This interaction can likely be tuned by variation of the electrode surface chemical composition, applied potential, wavelength of light, and plasmon resonance energy level (which can be shifted through the electrode surface geometry and material). Our results strongly suggest that understanding the influence of plasmon resonance energy alignment with charge injection energy levels may provide further guidance toward optimal plasmonic catalyst design. The possibility of achieving selectivity via plasmonic hot-carrier injection is particularly important for CO_2 reduction on hydrocarbon-producing composite photocatalysts such as Ag-Cu, which can produce a range of hydrocarbon products, such as CH_4, C_2H_4, and C_2H_6O.[33] Further studies, including potential-dependent CO_2 reduction product analysis, are needed to determine which mechanism is responsible for the observed catalysis. Future studies could also increase the area density of plasmonic structures to see an even more pronounced photocurrent effect.

Importantly, this concept can be extended to any electrochemical reaction limited by high overpotentials, where the interaction between the energy of plasmonic hot-carriers and intermediate molecules can be controlled at the molecular level. The hot-carrier injection to MOs or plasmonically induced strong local electric fields might additionally tune the binding energy of acceptors on a catalyst surface,[14,34] opening new mechanistic pathways. Thus, plasmonically excited hot-carriers are a promising new approach to overcome kinetic barriers of challenging electrochemical reactions and potentially improve their selectivity and faradaic efficiency.

6. Experimental Section

Nanopyramid Electrode Fabrication: A circular glass substrate (19 mm diameter and 0.5 mm thick, ProSciTech) was cleaned using acetone and isopropyl alcohol followed by washing in ultrapure water (Milli-Q) and then exposure to air plasma for 3 min. The air plasma cleaning enhances the adhesion of metals on the glass. A thin film of Ag/Ti (30 nm/3 nm) was deposited using an e-beam evaporator through a shadow mask having a dumbbell-like shape (see the Supporting Information). This thin film Ag electrode was tested as the "smooth" Ag electrode, and it was used as the base for deposition of nanopyramids.

A solution was prepared by mixing 20 mL of aqueous 1.7% (v/v) polystyrene (PS) bead suspension with 10 µL of 4% (v/v) Triton X-100. 740 nm diameter PS beads (Thermo-Scientific 5074A) or 310 nm diameter PS beads (Thermo-Scientific 5031A) were used to prepare water suspensions. A monolayer of close-packed PS beads was deposited on the Ag/Ti/glass substrate by withdrawing the substrate from the PS suspension at a 45° angle at a rate of 50 µm min^{-1}.[22,35] The layer of PS beads was used as a mask for Ag e-beam evaporation. The PS close-packed bead film has triangular openings into which the nanopyramids form during Ag deposition. To enlarge the openings in the 310 nm PS beads the film was etched by O_2 plasma for 270 s at 150 W.[36]

The optimal Ag deposition thickness that filled the apex of the pyramid without covering the beads was determined after several trials. 75 nm of Ag was deposited over the 310 nm polystyrene beads and 180 nm of Ag was deposited over the 740 nm beads. The polystyrene beads were then dissolved in tetrahydrofuran leaving behind 75 or 180 nm Ag nanopyramids arranged in a hexagonal pattern on a Ag film. 75 nm AgPyr has approximately fivefold higher density of nanopyramids per Ag-base surface area than 180 nm AgPyr.

Photoelectrochemical Measurements: Three different aqueous electrolytes were used in this study: 1) CO_2-saturated 0.1 M sodium perchlorate ($NaClO_4$, Alfa Aesar 98–102%) (pH = 4.1), 2) Ar-saturated 0.1 M $NaClO_4$ (pH = 9.1), and 3) 1 M sodium nitrate ($NaNO_3$, Sigma-Aldrich >99%) (pH = 5.7). All chemicals were used without further purification. Solutions were made using 18 MΩ purified water (Millipore system). The electrolyte was purged with CO_2 or Ar (Praxair 5.0 grade, purifier from Valco Instruments Co. Inc.) along with vigorous stirring for 30 min prior to the experiment. Electrochemical measurements were conducted in a single-compartment three-electrode glass cell fitted with a quartz window. An Ag/AgCl 3 M KCl (BASi) was used as the reference electrode and a platinum wire served as the counter electrode.

The working electrode potential was controlled by an SP-300 (Bio-Logic) potentiostat. All potentials presented here are referred to the RHE. LSV scans were performed at 5 mV s^{-1} while stirring and continuously bubbling the appropriate gas. A working electrode was illuminated by 300 W Xe lamp (Oriel) mechanically modulated at a frequency of 3 Hz. The total light density on the sample was measured to be ≈850 mW cm^{-2}. The potentiostat was connected to a lock-in amplifier (SRS 850) to extract the photocurrent generated by the intermittent light. The "dark" current and photocurrent densities were calculated with regard to the geometric surface area (0.5 cm^2), which is identical to the cross section of light incident on the surface.

Supporting Information

Supporting Information is available from the Wiley Online Library or from the author.

Acknowledgements

The authors thank Dr. Fen Qiu, Prof. Harry Atwater, Dr. David Srankó, Dr. Yanwei Lum, Dr. Guiji Liu, Ezra Clark, Dr. Jason Cooper, Dr. Ashely Gaulding, Dr. Hyo Won Kim, Dr. Chang-Ming Jiang, Jeff Beeman, David Larson, Aya Buckley, Dr. Alejandro Garza, and Dr. Jason Forster for useful discussions. This material is based upon work performed by the Joint Center for Artificial Photosynthesis, a U.S. Department of Energy Innovation Hub, supported through the Office of Science of the U.S. Department of Energy under Award No. DE-SC0004993. Work at

the Molecular Foundry was supported by the Office of Science, Office of Basic Energy Sciences, of the U.S. Department of Energy under Contract No. DE-AC02-05CH11231. E.B.C. and E.R.C. acknowledge support from the National Science Foundation Graduate Research Fellowship under Grant No. DGE 1106400.

Conflict of Interest

The authors declare no conflict of interest.

Keywords

Ag electrodes, CO_2, NO_3^- reduction, photo-electrocatalysis, surface plasmons

[1] a) Y. Hori, in *Modern Aspects of Electrochemistry*, Vol. *42* (Eds: C. G. Vayenas, R. E. White, M. E. Gamboa-Aldeco), Springer, New York **2008**, p. 89; b) K. P. Kuhl, E. R. Cave, D. N. Abram, T. F. Jaramillo, *Energy Environ. Sci.* **2012**, *5*, 7050.

[2] a) N. S. Lewis, D. G. Nocera, *Proc. Natl. Acad. Sci. USA* **2006**, *103*, 15729; b) C. W. Li, J. Ciston, M. W. Kanan, *Nature* **2014**, *508*, 504; c) E. E. Benson, C. P. Kubiak, A. J. Sathrum, J. M. Smieja, *Chem. Soc. Rev.* **2009**, *38*, 89; d) C. Costentin, M. Robert, J.-M. Savéant, *Chem. Soc. Rev.* **2013**, *42*, 2423.

[3] J. Shen, R. Kortlever, R. Kas, Y. Y. Birdja, O. Diaz-Morales, Y. Kwon, I. Ledezma-Yanez, K. J. P. Schouten, G. Mul, M. T. M. Koper, *Nat. Commun.* **2015**, *6*, 1.

[4] P. G. Russell, N. Kovac, S. Srinivasan, M. Steinberg, *J. Electrochem. Soc.* **1977**, *124*, 1329.

[5] Y. Hori, K. Kikuchi, S. Suzuki, *Chem. Lett.* **1985**, *14*, 1695.

[6] a) Y. Hori, A. Murata, K. Kikuchi, S. Suzuki, *J. Chem. Soc., Chem. Commun.* **1987**, *0*, 728; b) P. Kedzierzawski, J. Augustynski, *J. Electrochem. Soc.* **1994**, *141*, L58.

[7] C. Janaky, D. Hursan, B. Endrodi, W. Chanmanee, D. Roy, D. Liu, N. R. de Tacconi, B. H. Dennis, K. Rajeshwar, *ACS Energy Lett.* **2016**, *1*, 332.

[8] C. Reller, R. Krause, E. Volkova, B. Schmid, S. Neubauer, A. Rucki, M. Schuster, G. Schmid, *Adv. Energy Mater.* **2017**, *7*, 1602114.

[9] D. B. Ingram, S. Linic, *J. Am. Chem. Soc.* **2011**, *133*, 5202.

[10] S. Linic, P. Christopher, D. B. Ingram, *Nat. Mater.* **2011**, *10*, 911.

[11] R. Sundararaman, P. Narang, A. S. Jermyn, W. A. Goddard, H. A. Atwater, *Nat. Commun.* **2014**, *5*, 1.

[12] a) P. Narang, R. Sundararaman, H. A. Atwater, *Nanophotonics* **2016**, *5*, 96; b) M. L. Brongersma, N. J. Halas, P. Nordlander, *Nat. Nanotechnol.* **2015**, *10*, 25; c) C. Boerigter, U. Aslam, S. Linic, *ACS Nano* **2016**, *10*, 6108; d) A. M. Brown, R. Sundararaman, P. Narang, W. A. Goddard, H. A. Atwater, *ACS Nano* **2016**, *10*, 957; e) A. Manjavacas, J. G. Liu, V. Kulkarni, P. Nordlander, *ACS Nano* **2014**, *8*, 7630.

[13] a) A. Marimuthu, J. W. Zhang, S. Linic, *Science* **2013**, *339*, 1590; b) S. Linic, U. Aslam, C. Boerigter, M. Morabito, *Nat. Mater.* **2015**, *14*, 567.

[14] S. Mukherjee, F. Libisch, N. Large, O. Neumann, L. V. Brown, J. Cheng, J. B. Lassiter, E. A. Carter, P. Nordlander, N. J. Halas, *Nano Lett.* **2013**, *13*, 240.

[15] L. Zhou, C. Zhang, M. J. McClain, A. Manavacas, C. M. Krauter, S. Tian, F. Berg, H. O. Everitt, E. A. Carter, P. Nordlander, N. J. Halas, *Nano Lett.* **2016**, *16*, 1478.

[16] H. W. Gao, C. Liu, H. E. Jeong, P. D. Yang, *ACS Nano* **2012**, *6*, 234.

[17] a) A. A. Peterson, F. Abild-Pedersen, F. Studt, J. Rossmeisl, J. K. Norskov, *Energy Environ. Sci.* **2010**, *3*, 1311; b) A. A. Peterson, J. K. Norskov, *J. Phys. Chem. Lett.* **2012**, *3*, 251.

[18] J. Rosen, G. S. Hutchings, Q. Lu, S. Rivera, Y. Zhou, D. G. Vlachos, F. Jiao, *ACS Catal.* **2015**, *5*, 4293.

[19] R. Kostecki, J. Augustynski, *Chem. Phys. Lett.* **1992**, *194*, 386.

[20] R. Kostecki, J. Augustynski, *J. Appl. Electrochem.* **1993**, *23*, 567.

[21] R. Kostecki, J. Augustynski, *J. Appl. Phys.* **1995**, *77*, 4701.

[22] G. H. Chan, J. Zhao, E. M. Hicks, G. C. Schatz, R. P. Van Duyne, *Nano Lett.* **2007**, *7*, 1947.

[23] T. Hatsukade, K. P. Kuhl, E. R. Cave, D. N. Abram, T. F. Jaramillo, *Phys. Chem. Chem. Phys.* **2014**, *16*, 13814.

[24] a) J. K. Sass, R. K. Sen, E. Meyer, H. Gerischer, *Surf. Sci.* **1974**, *44*, 515; b) H. Neff, J. K. Sass, H. J. Lewerenz, *Surf. Sci. Lett.* **1984**, *143*, L356.

[25] Y. Kim, D. D. Torres, P. K. Jain, *Nano Lett.* **2016**, *16*, 3399.

[26] R. Kostecki, J. Augustynski, *Ber. Bunsen. Phys. Chem.* **1994**, *98*, 1510.

[27] Y. Y. Gurevich, Y. V. Pleskov, Z. A. Rotenberg, *Photoelectrochemistry*, Plenum Publishing Corporation, New York **1980**.

[28] F. W. Richey, B. D. McCloskey, A. C. Luntz, *J. Electrochem. Soc.* **2016**, *163*, A958.

[29] J. Krista, M. Kopanica, L. Novotny, *Electroanalysis* **2000**, *12*, 199.

[30] M. Fedurco, P. Kedzierzawski, J. Augustynski, *J. Electrochem. Soc.* **1999**, *146*, 2569.

[31] a) N. J. Firet, W. A. Smith, *ACS Catal.* **2017**, *7*, 606; b) S. Taguchi, J. M. Feliu, *Electrochim. Acta* **2008**, *53*, 3626.

[32] L.-Y. Hsu, W. Ding, G. C. Schatz, *J. Phys. Chem. Lett.* **2017**, *8*, 2357.

[33] D. Kim, J. Resasco, Y. Yu, A. M. Asiri, P. D. Yang, *Nat. Commun.* **2014**, *5*, 1.

[34] P. Avouris, R. E. Walkup, *Annu. Rev. Phys. Chem.* **1989**, *40*, 173.

[35] M. Tabatabaei, A. Sangar, N. Kazemi-Zanjani, P. Torchio, A. Merlen, F. Lagugne-Labarthet, *J. Phys. Chem. C* **2013**, *117*, 14778.

[36] L. Li, T. Y. Zhai, H. B. Zeng, X. S. Fang, Y. Bando, D. Golberg, *J. Mater. Chem.* **2011**, *21*, 40.